An Operational Near-Infrared Fluorescence Imaging System Prototype for Large Animal Surgery

Alec M. De Grand, B.S.[1]
John V. Frangioni, M.D., Ph.D.[1,2,3,*]

[1]Division of Hematology/Oncology

[2]Department of Radiology

[3]Molecular Imaging Group

Beth Israel Deaconess Medical Center

SL-B05, 330 Brookline Avenue

Boston, MA 02215

www.tcrt.org

Near-infrared (NIR) fluorescence imaging has the potential to revolutionize human cancer surgery by providing sensitive, specific, and real-time intraoperative visualization of normal and disease processes. We have previously introduced the concept of a low-cost, safe, and easy-to-use NIR fluorescence imaging system that permits the surgeon to "see" surgical anatomy and NIR fluorescence simultaneously, non-invasively, with high spatial resolution, in real-time, and without moving parts [Nakayama *et al. Molecular Imaging 1*, 365-377 (2002)]. In this study, we present an operational prototype designed specifically for use during large animal surgery. Such a system serves as a foundation for future clinical studies. We discuss technical considerations, and provide details of the implementation of subsystems related to excitation light, light collection, computer, and software. Using the prototype, and the clinically available NIR fluorophore indocyanine green, we demonstrate vascular imaging in 35 kg pigs. Cancer-specific applications of this imaging system include image-guided cancer resection with real-time assessment of surgical margins, image-guided sentinel lymph node mapping, intraoperative mapping of tumor and normal vasculature, image-guided avoidance of critical structures such as nerves, and intraoperative detection of occult metastases in the surgical field. Taken together, this study describes an optical imaging system engineered for eventual translation to the clinic.

Key words: Near-Infrared Fluorescence, *In Vivo* Imaging, Intraoperative Imaging, Large Animal Surgery.

Introduction

Even in 2003, cancer is a surgical disease. Of the 1.3 million non-skin cancers diagnosed each year in the United States, 50% are cured by surgical resection, approximately 5% are cured by chemotherapy and/or radiotherapy, and the remainder are incurable (1). Surprisingly, surgical resection of cancer has not changed significantly in the last century. Cancer surgery continues to be performed "blindly," without intraoperative confirmation of tumor extension, sensitive detection of microscopic metastases, mapping of tumor vasculature, or real-time confirmation that resection is complete.

There are several reasons why intraoperative imaging of cancer has not been pursued vigorously. The first reason is that an optimal imaging modality is not presently available to the surgeon. Angiography with iodine dyes permits mapping of vasculature, but requires exposure of patient and caregivers to x-rays, and exposure of the patient to millimolar concentrations of nephrotoxic iodine. Ultrasound is gaining popularity in the OR, but has poor sensitivity and specificity for tumor detection, and presently few ultrasound contrast agents have been described. Magnetic resonance imaging (MRI) offers superb anatomical information, but to date, contrast methods are insensitive, few target-specific contrast agents have been

* Corresponding Author:
John V. Frangioni, M.D., Ph.D.
Email: jfrangio@bidmc.harvard.edu

described, and instrument bulkiness precludes its use in many surgical procedures. Radioscintigraphy with mid-level gamma-ray emitters such as ^{99m}Tc is being used more frequently, but detection methods such as single photon emission computed tomography (SPECT) are not suitable for the space and time constraints of human surgery.

The second major reason that intraoperative imaging is not performed routinely is cost. Angiography and MRI require modifications to the operating room that can cost millions of dollars, and both types of imaging systems require dedicated technicians. SPECT radioscintigraphy is also quite costly, and not suitable for the operating room. Although ultrasound is less expensive, it is also less useful for most procedures.

The third major reason that intraoperative imaging is not performed routinely is the lack of availability of cancer-specific contrast agents. Even if the above imaging modalities were sensitive, practical, and inexpensive, the field of cancer-specific targeting molecules is only now blossoming. A recent review summarizes contrast agents available for near-infrared fluorescence imaging (2).

The fourth, and some might argue, most important reason why intraoperative imaging of cancer is not performed routinely in the United States is the difficulty in transferring new technology to the community setting. Hence, an ideal intraoperative imaging system would be highly sensitive and specific, relatively inexpensive, safe to use, and easy to use. To date, no such imaging system meets these criteria.

Our long-range goal is to develop a near-infrared (NIR) fluorescence optical imaging system for use during human surgery. The use of near-infrared wavelengths for imaging permits relatively deep photon penetration into tissue, minimal autofluorescence, less scatter, and high optical contrast when exogenous NIR fluorophores are introduced. The technology we describe in this study is, in effect, an extension of the human eye, embellishing what the surgeon is used to seeing by providing functional information obtained using exogenous NIR fluorescent contrast agents (3). The end result is sensitive, specific, and real-time intraoperative imaging system. The technology is relatively inexpensive, has no moving parts, does not touch the subject, exposes the subject only to low fluence rate light, and has been made extremely easy to use.

Materials and Methods

Mechanical Subsystem

The steel cart housing the imaging system was custom built by Mobile-Tronics (Mission Viejo, CA). The base plate (Catalog # 5164T51) and 12" straight extension (Catalog # 5164T62) for the articulating arm (Catalog # 5164T72) were purchased from McMaster-Carr (New Brunswick, NJ). A custom aluminum adapter plate (Micro Video Instruments, Avon, MA) attached the articulating arm to the excitation/emission module. Surge suppression was provided by a model F5H300-EXT 20 A outlet (Belkin, Compton, CA) attached to the interior of the cart.

Excitation Light Subsystem

White light was generated by a model PL-900F 150 W halogen source (Dolan-Jenner, Lawrence, MA) that was depleted of NIR- and IR-wavelengths using three layers of filtration. First, the permanent internal heat glass was replaced with a 25 mm diameter, 3.3 mm thick extended range hot mirror (catalog #NT-46-386, Edmund Industrial Optics, Barrington, NJ), oriented with the reflective surface towards the bulb. Second, the model IR-1 heat filter provided with PL-900F filter holder was used. Third, a custom aluminum hot mirror holder/adapter (model IR-5500/590, R. J. Wilson Associates, Weymouth, MA) was machined such that its 1" diameter end fit into the nosepiece of the PL-900F. A second round hot mirror (same as above) was ground to mount in this adapter. The other end of the adapter had a 0.590" opening into which the ringlight fiber bundle was inserted. The adjustable working distance ringlight, with a 62" long fiber bundle (0.32" diameter glass, 0.59" outer diameter), catalog #RL040103, was purchased was from Thales-Optem (Fairport, NY).

For NIR fluorescence excitation light, a model A-240-D (Dolan-Jenner) dual 150 W halogen source was used with the following modifications made by R. J. Wilson Associates. For each illuminator, the bulb holder was bent to be perpendicular to the lamp nosepiece. The internal baffle/filter holder was removed. The nosepiece was modified to mount a 25 mm diameter Nikon filter excitation ring using setscrews. The rubber feet were removed and the housings secured to an aluminum plate. The plate, in turn, was mounted to the excitation/emission coupler via a model FA-1 articulating arm (R. J. Wilson Associates). Finally, the face of the illuminator was sealed with aluminum tape to eliminate light leakage. EJV bulbs were chosen over EKE bulbs based on a slightly higher output in the NIR. NIR fluorescence excitation light was filtered using a 25 mm diameter 725-775 nm bandpass filter (catalog #HQ750/50, Chroma Technology, Brattleboro, VT) glued using black RTV silicon to a Nikon (Melville, NY) excitation filter ring.

Light Collection Optics and Filtration

Light from the surgical field was collected using a custom zoom lens system with an 18" working distance (Thales-Optem, Fairport, NY). The zoom lens was mounted to a custom camera coupler/filter cube holder (Thales-Optem). The dichroic mirror (Chroma catalog #785dcxr-special) was per-

manently mounted in a Nikon TE 300 filter cube (catalog #91001). The 25 mm diameter color video camera cleanup filter (catalog #E680SP, Chroma) was glued as above into a Nikon excitation filter ring. The 25 mm diameter fluorescence emission filter (catalog #HQ810/40, Chroma) was similarly glued into a Nikon emission ring. The rings, in turn, were mounted to the filter cube as described below. Cameras were mounted to the coupler via C-mount optics.

Cameras and Frame Grabbers

For recording of color video images, a Hitachi (Tarrytown, NY) model HV-D27 three-chip CCD camera was connected to a model PCI-1411 S-video frame grabber (National Instruments, Austin, TX) using an S-video cable. For recording of NIR fluorescence images, a Hamamatsu (Bridgewater, NJ) model Orca-ER interline CCD camera was connected to a model PCI-1422 frame grabber (National Instruments) using a National Instruments catalog #185232-02 cable. Cameras were purchased from Micro Video Instruments. Frame grabbers were purchased from Graftek Imaging (Austin, TX).

Computer and Software

Computer control and data acquisition were performed with a 2.4 GHz Pentium 4 Precision Workstation 340 (Dell, Round Rock, TX) equipped with 512 MB memory, SCSI (10,000 rpm) hard disk drive, 17-inch (1280 × 1024 pixel) monitor and Windows 2000. All control software was written in LabVIEW version 6.1 and IMAQ Vision version 6.1, with Measurement and Automation version 3.0 used for hardware debugging (National Instruments). To improve system performance, the Orca-ER IDC supplied with LabVIEW was modified to remove serial control delays and permit subarray acquisition. All software was purchased from Graftek Imaging. For footswitch control, the 4 TTL lines available on the PCI-1422 board were accessed using a National Instruments catalog #185298-01 DB25 to BNC breakout cable. A custom footswitch box contained three SPST momentary switches utilizing 10 kΩ pull-up resistors.

Vascular Imaging of the Pig Heart

Yorkshire pigs (35 kg) were purchased from EM Parsons (Hadley, MA) and were used in accordance with an approved institutional protocol. Pigs were induced with 4.4 mg/kg intramuscular Telazol (Fort Dodge Labs, Fort Dodge, IA) and anesthesia was maintained through a 7 mm endotracheal tube with 1.5% isoflurane/98.5% O_2 at 5 L/min. For vascular imaging of the heart, a midline thoracotomy was performed, and 2 mg of the NIR fluorophore indocyanine green (ICG; Akorn, Decatur, IL), resuspended in 0.5 ml saline, was injected intravenously (final concentration 0.057 mg/kg). Time-lapse image acquisition in Cine mode was performed at 2 Hz throughout the procedure.

Results

Principle of Operation

We have previously published the concept of simultaneous intraoperative imaging of visible reflected light and NIR fluorescence emitted from exogenously administered contrast agents (3). The core technology used by this imaging system exploits the sensitivity curve of the human eye (Figure 1A). Even under high light level (photopic) conditions, the human eye has poor sensitivity to wavelengths greater than 700 nm (4, 5). Under low light level (scotopic) conditions, sensitivity to these wavelengths is more than two logs lower (6). Hence, it is possible to simultaneous irradiate a surgical field with visible light (400 nm to 700 nm) and NIR excitation light, with
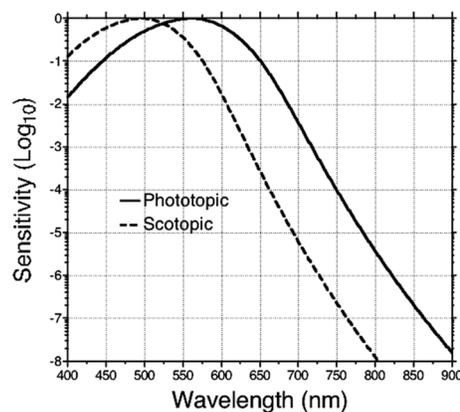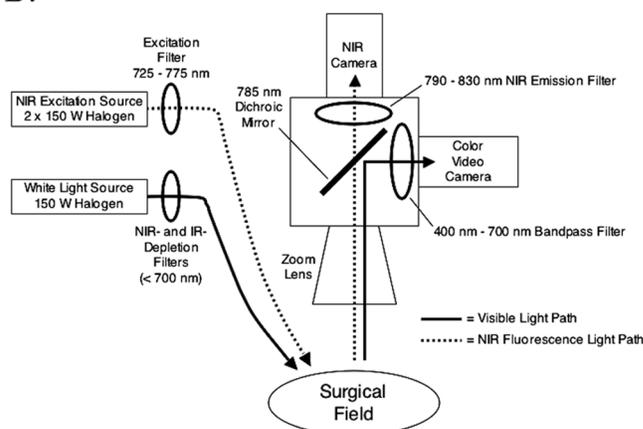
Figure 1: Overview of imaging system technology. **A.** Spectral sensitivity curve of the human eye as a function of wavelength. Typical environmental fluence rates range from low light conditions (scotopic) to high light conditions (photopic). Shown are the data points of (4, 5) (photopic) and (6) (scotopic) plotted using the equation of (33). **B.** Simultaneous color video/NIR fluorescence intraoperative imaging system. The NIR light path (dotted lines) is optically isolated from the visible (NIR-depleted) light path (solid lines) by use of separate excitation sources, a dichroic mirror, and barrier filters. All system components are under computer control. Adapted from (3, 8).

Table I
Prototype Imaging System Specifications

Physical (Cart)	
Size:	27" W x 27" D x 40" H
Weight:	245 lbs.
Power Source:	110 V AC, Surge-Suppressed, 10 Outlets, 20 A Max
Physical (Excitation/Emission Module)	
Size:	18" W x 5" D x 24" H
Weight:	≈ 14 lbs.
Optics and Display	
Working Distances:	8 " (NIR Excitation Light Sources)
	18" (NIR/IR-Depleted White Light Source and Optics)
Surgical Field of View:	4 W x 3 H cm to 20 W x 15 H cm (Adjustable)
Monitor Pixel Resolution:	1280 W x 1024 H Minimum
Image Windows:	Color Video, NIR Fluorescence, Pseudocolored Merge
Image Pixel Resolution:	640 W x 480 H per Image Window
System Resolution:	125 μm (x,y) to 625 μm (x,y)
Display Refresh:	15 Hz Maximum (for All Three Windows)
NIR Fluorescence Image Integration Time:	10 msec to 10 sec
Excitation/Emission Module	
Illuminated Area:	20 cm Diameter
NIR Excitation Light Source:	2 x 150 W Halogen
NIR Excitation Light Wavelength Range:	725 - 775 nm
NIR Excitation Light Fluence Rate:	0 - 5 mW/cm^2 (adjustable)
NIR Fluorescence Emission Filtration:	790 - 830 nm bandpass
White Light Source:	150 W Halogen
White Light Source Wavelength Range:	< 700 nm
White Light Fluence Rate:	0 - 0.5 mW/cm^2 (adjustable)
User Interface	
Software:	LabVIEW v. 6.1 and IMAQ Vision v. 6.1
Surgeon Controls:	Footswitches and/or Keyboard

the NIR light being "invisible" to the surgeon (Figure 1B). By maintaining separation of the visible (i.e., color) and NIR fluorescent light (Figure 1B), it is possible to simultaneously acquire color (i.e., surgical anatomy) and NIR fluorescence (i.e., vessel location, nerve location, tumor location, etc.) images, and to overlay the two in real-time (examples given below). Moreover, the imaging system we describe in this study has no moving parts, no contact with the patient, and working distances that ensure sterility of the surgical field. A complete list of its specifications is provided in Table I.

Ergonomics and Portability

To accommodate most operating rooms (ORs), the imaging system is completely self-contained within a 27" H × 27" D × 40" H, custom-designed steel cart with 4 rotating and locking wheels (Figure 2A and Table I). Cart doors are held open using magnets, and when closed, can provide locked storage for all imaging system components. The top of the cart was reinforced for attachment of a steel articulating arm with 360º freedom of rotation. To the articulating arm is mounted the aluminum plate housing the excitation/emission module (Figures 2A and 2B). The excitation/emission module has 270º of rotation around the axis of the arm. The arm is counterbalanced using a tension spring so that minimal force

is required to position the excitation/emission module over the surgical field. The only external attachment to the cart is the 110 V AC plug emanating from the 10-outlet surge suppressor. Deployment of the imaging system during actual large animal surgery is shown in Figures 3A and 3B.
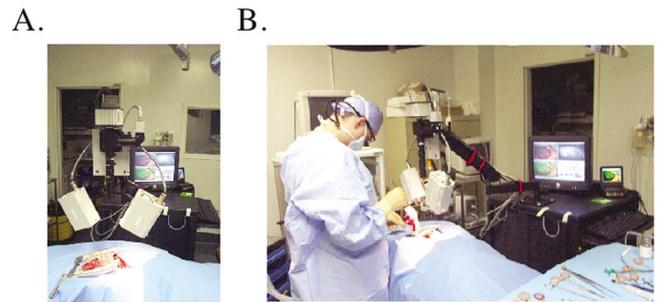
Excitation/Emission Module

Large animal and human surgery introduce requirements and constraints not encountered during small animal intraoperative imaging. In particular, the field of view (FoV) of the surgical field must be adjustable from as little as 4 cm in width to as much as 20 cm in width, depending on the surgical procedure and required resolution. To permit simultaneous acquisition of color video and NIR fluorescence images, the white light source illuminating the surgical field is depleted of all NIR and IR wavelengths (675-1700 nm) using the filtration described in ***Materials and Methods*** (see also Figure 4A). The combination of a single 150 W filtered halogen source and an adjustable working distance ringlight (Figure 2B) generated white light fluence rates averaging 0.5 mW/cm^2 over a 20 cm diameter fixed illumination area.

For NIR fluorescence excitation over the same area, we chose to use two 150 W halogen sources, filtered to 725-775 nm as
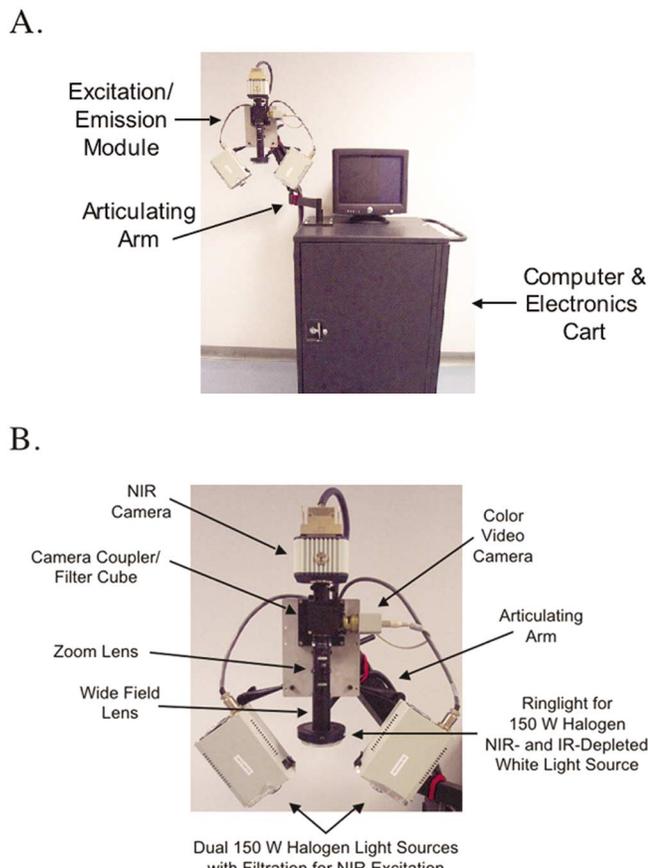
Figure 2: Prototype intraoperative NIR fluorescence imaging system for large animal surgery. **A.** In the closed configuration (shown), the imaging system is completely mobile. All computer and electronics reside in a steel cart with locking wheels. The excitation/emission module (see also Figure 2B) is connected to the cart via a counter-balanced articulating arm. **B.** Excitation/Emission module. All system optics are contained within the excitation/emission module. Fluorescence excitation light (725-775 nm) is supplied over a 20-cm diameter surgical field using two 150 W halogen sources equipped with custom filtration. The position of the sources is adjustable via articulated arms. NIR- and IR-depleted white light is supplied by an adjustable fiberoptic ringlight connected to a 150 W halogen source. Light reflected from the surgical field is collected by wide field and zoom lenses, and passes through the filter cube and camera coupler, where NIR fluorescence emission and reflected white light are directed to their respective cameras (see Figure 1B for operational schematic).

described in ***Materials and Methods***. Halogen was chosen over xenon, metal halide, and mercury sources since bulb output is easily controlled electronically. NIR lasers were purposely avoided for two reasons: safety and cost. To generate even 5 mW/cm^2 over a 20 cm diameter FoV, a 1.5 W, class IV continuous wave (CW) laser would be needed. This would necessitate all personnel in the room to wear protective eyewear, and an interlocked power source. The cost of such a high power laser would also be significant compared to filtered broadband sources. The halogen sources were mounted on either side of the surgical field, using articulating arms, to minimize inhomogeneities and shadowing (Figure 2B). Although this configura-

Figure 3: Deployment of the NIR fluorescence imaging system in the operating room. **A.** View of the imaging system as seen by the surgeon. The excitation/emission module, on a counterbalanced articulating arm, resides 12-18" above the surgical field and can be moved in any direction as needed. Images are displayed on a monitor residing on the cart, or alternatively, a satellite monitor attached directly to the excitation/emission module (not shown). **B.** Use of the imaging system during cardiothoracic surgery of the pig.
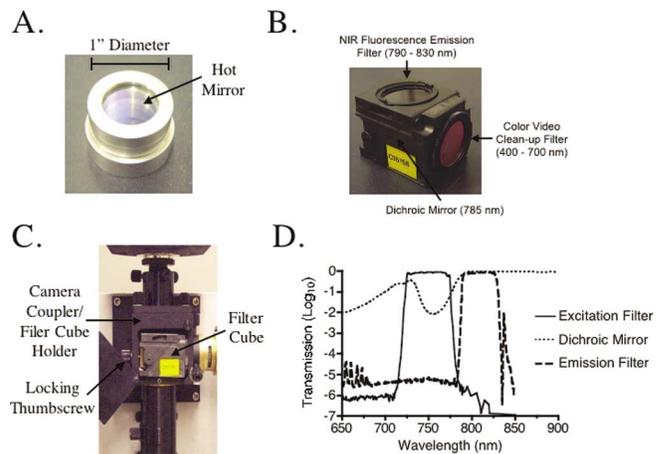
Figure 4: Excitation light filtration. **A.** The NIR- and IR-depletion filter adapter (<700 nm) for the white light source fits into the standard 1" nosepiece of Dolan-Jenner fiberoptic light sources. **B.** The Nikon TE-300 filter cube, used in the inverted position, permits redirection of reflected white light and NIR fluorescence light to their respective cameras. **C.** The filter cube slides into the light-tight camera coupler and is locked in place with a thumbscrew. **D.** Transmission properties of the NIR excitation filter (725-750 nm), dichroic mirror (785 nm center wavelength), and NIR emission filter (790-830 nm).

tion was capable of generating 5 mW/cm^2 of NIR excitation light over a 20 cm diameter surgical field, a significant disadvantage was that maximum distance between source and surgical field was only 8". Another disadvantage was that the necessary placement of the excitation filters close to the halogen bulbs produced heat damage to the filters after approximately 30 hours of use.

System optics also require attention to detail. A minimum number of lens surfaces were employed, and all lenses were selected based on excellent NIR transmission. Light emanating from the surgical field is split into color video and NIR fluorescence emission components using a dichroic mirror mounted in a standard Nikon TE300 microscope filter cube (Figure 4B; ***Material and Methods***). This cube can be changed rapidly for use of the system with different fluo-

rophores. To accommodate our application, the cube is used in an inverted position (Figure 4B) such that the "excitation" filter is actually the clean-up filter for the color video camera (to exclude NIR excitation and emission light) and the dichroic mirror transmits NIR fluorescence emission light to a separate bandpass filter. The dual camera coupler was engineered to accept this cube into a light-tight holder, and to lock it in place via a plate and thumbscrew (Figure 4C). The transmission properties of the NIR excitation filter, dichroic mirror, and NIR emission filter are shown in Figure 4D. The color video and NIR cameras attached to the camera coupler/filter holder using standard C-mount connections, and both cameras could be independently aligned, magnified, and focused to permit perfect overlap of the color video and NIR fluorescence images, and to correct for chromatic aberrations in the two light paths.

The color video camera chosen (Hitachi HV-D27), although expensive, is a highly sensitive 1/2" 3-chip camera with excellent color reproduction and auto-gain function. Although capable of 640 × 480 RGB output at 30 Hz, its S-video output was used due to limitations in the availability of RGB frame grabbers supported by LabVIEW. The NIR fluorescence CCD camera chosen (Hamamatsu Orca-ER; 2/3" format) has reasonable quantum efficiency at 800 nm (≈ 30-35%), and has interlined output achieving 15.8 Hz at 640 × 480 resolution (using 2 × 2 binning with subarray sampling). Although a gallium arsenide-based detector might achieve a higher quantum efficiency, this particular cooled silicon CCD camera offers an excellent price to performance ratio, low noise, and is easily interfaced with LabVIEW.

Computer and Software

A single 2.4 GHz Pentium 4 workstation controls the entire system, with its frame grabbers and cabling described in detail in ***Materials and Methods***. A key feature of the intraoperative NIR fluorescence imaging system is its control software and user interface. The exact monitor view seen by the surgeon is shown in Figure 5A. In the upper left corner of the screen is a 640 × 480 pixel window displaying the color video image of the surgical field. In the upper right corner of the screen is the 640 × 480 12-bit NIR fluorescence emission image of the same field rendered in 8-bit monochrome. In the bottom left corner of the screen is the merged image of the color video window and NIR fluorescence emission window, with the latter rendered in an unnatural pseudocolor (lime green in the example) and overlaid with a user-controlled opacity. Lime green is particularly useful for the pseudocolored merged image since it provides high color contrast with living tissue. In the bottom right corner of the screen is the user interface. All windows are refreshed at a maximum of 15 Hz (a function of the NIR camera), although NIR fluorescence integration time is selectable from 10 msec to 10 sec.

A.
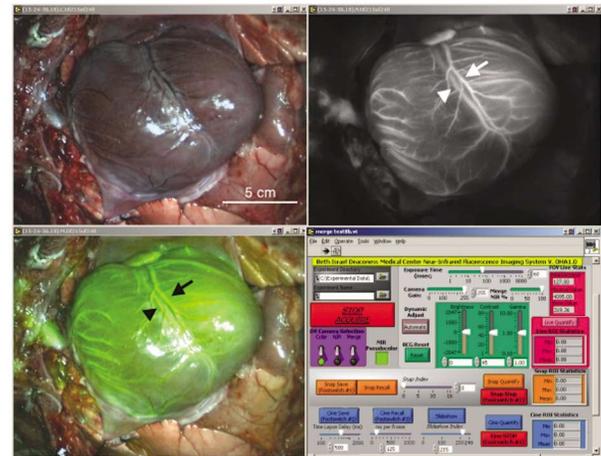
B.
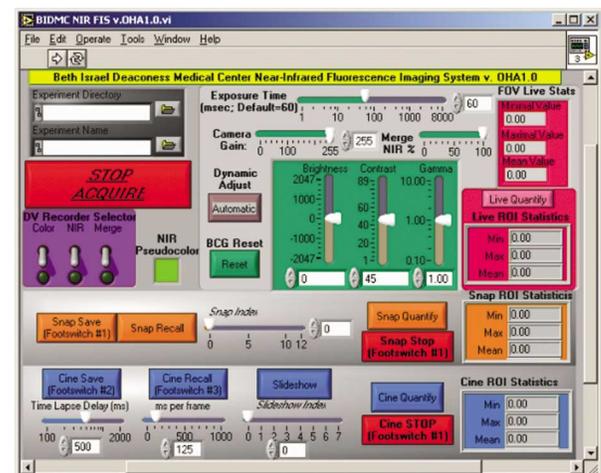
Figure 5: Imaging system software, monitor display, and user interface. **A.** Imaging system monitor display. Shown is the exact monitor display seen by the surgeon. The top-left quarter of the screen is the color video image (i.e., what the surgeon is used to seeing). In the top-right quarter of the screen is the otherwise-invisible NIR fluorescence image. In the bottom-left quarter of the screen is the pseudo-colored overlay of the NIR fluorescence (lime green) and color images, and in the bottom-right quarter is the imaging system control panel. The images shown are the actual data acquired during intravascular mapping of the coronary circulation, using indocyanine green, in a 35 kg pig. Positions of the arterial system (arrow) and venous system (arrowhead) are shown. A scale bar has been added to the figure for heart size reference. **B.** Imaging system control panel. The user interface, created with the LabVIEW programming environment, provides the surgeon with complete control over the imaging system, include camera gain and exposure time, quantitation of all images, static (Snap) and dynamic (Cine) data acquisition, and image display characteristics (e.g., brightness, contrast, gain, and NIR fluorescence pseudocolor for overlay with the color image).

As shown in Figure 5B, the user interface provides the surgeon with complete control over camera functions, data acquisition, image display, and data archiving. The system operates in three modes. In free running mode, the display is refreshed at a rate set by the camera exposure time. In Snap acquire mode,

a single frame of color video, NIR fluorescence, and merged images are saved to the hard disk. In Cine acquire mode, a continuous time lapse of all three image windows is saved to the hard disk at a sampling frequency determined by a slider control. Data are saved in 24 bit color (color video and merged images) and 12-bit monochrome (NIR fluorescence image) formats. Brightness, gain, and contrast of the NIR image can be adjusted automatically or manually. For Snap and Cine operating modes, data acquisition is triggered via keyboard or footswitch. Saved images can be quickly retrieved in an indexed (Snap mode) or slideshow (Cine mode) format. Cine images can also be replayed as a movie, with the replay rate set by a slider. All three modes permit quantification of the NIR fluorescence images using arbitrarily-sized regions of interest (ROI), with statistics such as minimum, maximum, and mean pixel value displayed for the ROI. For long surgeries where only a single window of acquisition is desired, the system can accommodate a scan converter (Corioscan Pro CS-500, TV One, Erlanger, KY) connected to a miniDV recorder (model GV-D900, Sony, New York, NY). The software is available from the authors as an executable file (.exe), although an IMAQ Vision run-time license (catalog #778044-00) must be purchased from National Instruments (through Graftek Imaging), and a free LabVIEW run-time engine must be downloaded from the National Instruments website (www.ni.com).

Intraoperative Vascular Imaging of Large Animals

The performance of the NIR fluorescence imaging system during large animal surgery is demonstrated in Figure 5A. After thoracotomy, NIR fluorescence angiography was performed in a 35 kg pig using the FDA-approved NIR heptamethine indocyanine fluorophore indocyanine green (ICG). ICG was injected at a dose of 0.057 mg/kg and Cine images were acquired as described in *Materials and Methods*. Shown in Figure 5A are data acquired during both arterial and venous filling. The signal to background ratio of the highlighted vessels was > 30:1. In both the NIR fluorescence and merged images, fine vascular mapping could be performed, and patency inferred by the adequacy of vessel contrast. During oncologic surgery, the imaging system would be expected to permit similar mapping of either normal or tumor vasculature, thus aiding in defining tumor extent, ensuring adequacy of resection, and assisting in avoidance of critical normal vessels.

Discussion

In this study, we present an operational NIR fluorescence imaging system prototype, and demonstrate its performance during angiography in a simple large animal model. The imaging system is truly a prototype, and several possible improvements are evident. For example, the use of halogen light sources, while inexpensive and effective for achieving adequate fluence rates over large surface areas, suffer from bulk, weight, overheating of filters, and the necessity to be ≤ 8" from the surgical field. The optics, on the contrary, have been designed to function optimally at least 18" from the surgical field. The use of alternative non-laser light sources is expected to improve system ergonomics, working distance, and performance significantly.

Just how much is "enough" fluorescence excitation light illuminating the surgical field is, at present, unanswered. For CW fluence rates above 50 mW/cm^2, the heptamethine indocyanines such as ICG, IR786, and IRDye78 photobleach rapidly (7). Hence, for most applications, it is likely that 50 mW/cm^2, is a reasonable maximum fluence rate. Indeed, higher fluence rates can also result in significant heating of tissue. For a 20 cm diameter FoV, a fluence rate of 50 mW/cm^2 (the NIR fluorophore photobleaching threshold) corresponds to 15 W of total NIR excitation light, which itself will be difficult to achieve with any light source. Nevertheless, for sensitive detection of tumors that may be relatively deep in tissue, it is expected that such a high fluence rate will be required.

A major limitation of the reflectance-type imaging system described in this study is the potentially poor performance, due to the combined effects of absorption and scatter, when the desired target is deeper than approximately 0.5 cm in tissue (discussed in (8, 9)). However, when "detection" rather than "imaging" is the goal, it is often possible to find targets deeper than 0.5 cm (10). The three surgeons who have operated with the imaging system over the last six months have found numerous surgical applications that benefit from it, despite its present limitations. Their studies are either in press (10) or in preparation (Soltesz *et al*.; Mihaljevic *et al*.; Parungo *et al*.; data not shown). Furthermore, each component of the imaging system has been designed in a modular fashion so that newer imaging techniques, such as frequency-domain photon migration (reviewed in (11, 12)), can be incorporated.

Cancer surgery is predicated on the removal of all malignant cells from the body. However, there is presently no method available to the surgeon to assess whether resection is complete, or whether occult metastases are present in the surgical field. For decades, intraoperative frozen section biopsy has been the only method used routinely for detecting the presence of cancer in a surgical specimen. In this technique, the surgeon freezes a small piece of tissue in liquid nitrogen, and a pathologist in the OR cryostats the specimen into ≈ 20 μm sections and views it under the microscope for the presence or absence of frankly malignant cells. As might be expected, this procedure is time consuming, expensive, relatively insensitive, and most importantly, introduces substantial sampling bias since the specimen examined is orders of magnitude smaller than the tissue being operated upon.

The four most prevalent cancers in the United States, breast, colon, lung, and prostate account for nearly 600,000 new cases each year. Prior to metastasis, each is curable by complete surgical resection. The following is a brief synopsis of how intraoperative NIR fluorescence imaging technology could potentially improve the outcomes of these surgeries.

Breast Cancer

The new standard of care in breast cancer surgery is the sentinel lymph node (SLN) biopsy. During this procedure, a mixture of radioactive tracer (e.g., Technetium-99m sulfur colloid) and blue dye (e.g., isosulfan blue) is injected around the tumor, and the SLN is identified and resected by using a combination of handheld gamma probe and surgical exploration to find the "blue" lymph node. Intraoperative NIR fluorescence imaging has the potential to replace both radioactivity and chromophoric dye (10, 13), while providing anatomical co-registration of tumor and anatomy, and real-time lymph node mapping. During the surgery itself, NIR fluorescent, breast cancer-specific targeting molecules could additionally be used to ensure that breast cancer resection is complete, and that all lymph nodes containing malignant cells are removed.

Colon Cancer

The prognosis of colon cancer depends to a large extent on lymph node involvement. Since epithelial cells should not otherwise be found in normal lymph nodes, NIR fluorescence imaging using an epithelial-specific marker such as CEA could assist the surgeon in identifying which nodes to sample during surgery, and could also be used to identify occult extension of the tumor. NIR fluorescent lymph node mapping could also prove useful in identifying which nodal basin should be sampled.

Lung Cancer

Even in Stage I lung cancer, surgical resection is less than 50% curative. This is due to a combination of local and distant metastases, and without intraoperative imaging of the tumor, it is not possible to determine whether small collections of cells are being left behind. Moreover, since lymph node drainage of the lung is extremely complex, intraoperative lymph node mapping using NIR fluorescent contrast agents may be useful in locating occult cancer.

Prostate Cancer

The radical prostatectomy has several technical limitations. In the nerve-sparing procedure, there is presently no method available for directly visualizing the nerves. Using a NIR fluorescent nerve-targeting molecule that shows the surgeon exactly where the nerves are located, the success of this procedure might be greatly improved. Moreover, during the

prostatectomy itself, NIR fluorescence imaging could be used to find prostate cancer cells that have metastasized to pelvic lymph nodes, and to ensure that surgical margins are negative.

Even cancers such as melanoma, previously considered incurable once metastatic, have been shown in three recent trials to have an improved survival after complete surgical resection and adjuvant vaccination (14-16). Here, too, sensitive and specific intraoperative imaging of the tumor(s) would be expected to result in an even greater improvement in surgical outcome.

The use of near-infrared light and exogenous contrast agents for surgical imaging has several inherent advantages. First, photon penetration into, and out of, the tissue is high. Second, tissue autofluorescence is low, so an inherently high contrast between target tissue and normal epithelium can be achieved. Third, optical scatter within tissue is lower, albeit significant, as compared to shorter wavelength visible light. Fourth, both organic and inorganic contrast agents spanning the entire NIR spectrum are readily available (2).

To date, a surprising number of exogenous NIR fluorophores, all of which are compatible with the intraoperative imaging system described in this study, have been used for *in vivo* imaging of animals and humans (reviewed in (2)). The FDA-approved NIR fluorophore indocyanine green has been used in research studies to image the vasculature of the human eye (17, 18), ophthalmic tumors (19), the human brain (20), canine mammary tumors (21), the gastrointestinal system (22), and human coronary arteries (23). Indocyanine green has also been used in humans to assess burn depth (24).

Improved hydrophilic NIR fluorophores have been used to image rat coronary arteries (3), and hydrophobic NIR fluorophores have been used as perfusion tracers for brown fat (7) and myocardium (3). Inorganic NIR fluorophores, such as quantum dots, have been used to image coronary vasculature (9) and sentinel lymph nodes (10). Finally, targeted and/or stealth NIR fluorophores, have been used to image the inflammation associated with coronary atherosclerosis (25), thrombin activation (26), dysplastic intestinal adenomas (27), cell death (28), hydroxyapatite (8), somatostatin receptors (29, 30) and folate receptors (31). There is no doubt that the list of application-specific NIR fluorophores will continue to grow as chemical obstacles are removed (32) and more investigators utilize the technology.

In summary, this study describes the development of a prototype intraoperative NIR fluorescence imaging system that can exploit novel contrast agents to provide the surgeon with unparalleled image guidance during complex surgical procedures. In the future, cancer resection could be performed while "seeing" the actual extent of the tumor, and while avoiding damage to normal tissue, such as nerves and blood vessels.

Sentinel lymph node mapping could be performed under real-time visualization of lymph flow. And, occult metastases in the surgical field could be identified before completing the surgery, thus ensuring that the surgeon "got it all out". In short, intraoperative NIR fluorescence imaging has the potential, as yet unproven, to revolutionize human cancer surgery.

1. *Surveillance, Epidemiology, and End Results (SEER) Database*. 1973-1999, National Cancer Institute.
2. Frangioni, J. V. *In Vivo* Near-infrared Fluorescence Imaging. *Curr. Opin. Chem. Biol. 7*, 626-634 (2003).
3. Nakayama, A., del Monte, F., Hajjar, R. J., Frangioni, J. V. Functional Near-infrared Fluorescence Imaging for Cardiac Surgery and Targeted Gene Therapy. *Molecular Imaging 1*, 365-377 (2002).
4. Goodeve, C. F. Relative Luminosity in the Extreme Red. *Proc. Royal Society A 155*, 664-683 (1936).
5. Griffin, D. R., Hubbard, R., Wald, G. The Sensitivity of the Human Eye to Infra-red Radiation. *J. Opt. Soc. America 37*, 546-554 (1947).
6. Crawford, B. F. The Scotopic Visibility Function. *Proc. Phys. Soc. B 62*, 321-334 (1949).
7. Nakayama, A., Bianco, A. C., Zhang, C. Y., Lowell, B. B., Frangioni, J. V. Quantitation of Brown Adipose Tissue Perfusion in Transgenic Mice Using Near-infrared Fluorescence Imaging. *Molecular Imaging 2*, 37-49 (2003).
8. Zaheer, A., Lenkinski, R. E., Mahmood, A., Jones, A. G., Cantley, L. C., Frangioni, J. V. *In Vivo* Near-infrared Fluorescence Imaging of Osteoblastic Activity. *Nat. Biotechnol. 19*, 1148-1154 (2001).
9. Lim, Y. T., Kim, S., Nakayama, A., Stott, N. E., Bawendi, M. G., Frangioni, J. V. Selection of Quantum Dot Wavelengths for Biomedical Assays and Imaging. *Molecular Imaging 2*, 50-64 (2003).
10. Kim, S., Lim, Y. T., Soltesz, E. G., De Grand, A. M., Lee, J., Nakayama, A., Parker, J. A., Mihaljevic, T., Laurence, *et al*. Near-infrared Fluorescent Type-II Quantum Dots for Sentinel Lymph Node Mapping. *Nat. Biotechnol*. In Press.
11. Sevick-Muraca, E. M., Houston, J. P., Gurfinkel, M. Fluorescence-enhanced, Near Infrared Diagnostic Imaging with Contrast Agents. *Curr. Opin. Chem. Biol. 6*, 642-650 (2002).
12. Ntziachristos, V., Bremer, C., Weissleder, R. Fluorescence Imaging with Near-infrared Light: New Technological Advances that Enable *In Vivo* Molecular Imaging. *Eur. Radiol. 13*, 195-208 (2003).
13. Josephson, L., Mahmood, U., Wunderbaldinger, P., Tang, Y., Weissleder, R. Pan and Sentinel Lymph Node Visualization Using a Near-infrared Fluorescent Probe. *Molecular Imaging 2*, 18-23 (2003).
14. Morton, D. L., Hsueh, E. C., Essner, R., Foshag, L. J., O'Day, S. J., Bilchik, A., Gupta, R. K., Hoon, D. S., Ravindranath, M., *et al*. Prolonged Survival of Patients Receiving Active Immunotherapy with Canvaxin Therapeutic Polyvalent Vaccine After Complete Resection of Melanoma Metastatic to Regional Lymph Nodes. *Ann. Surg. 236*, 438-448 (2002).
15. Hsueh, E. C., Essner, R., Foshag, L. J., Ollila, D. W., Gammon, G., O'Day, S. J., Boasberg, P. D., Stern, S. L., Ye, X., Morton, D. L. Prolonged Survival After Complete Resection of Disseminated Melanoma and Active Immunotherapy with a Therapeutic Cancer Vaccine. *J. Clin. Oncol. 20*, 4549-4554 (2002).
16. Chung, M. H., Gupta, R. K., Hsueh, E., Essner, R., Ye, W., Yee, R., Morton, D. L. Humoral Immune Response to a Therapeutic Polyvalent Cancer Vaccine After Complete Resection of Thick Primary Melanoma and Sentinel Lymphadenectomy. *J. Clin. Oncol. 21*, 313-319 (2003).
17. Herbort, C. P., LeHoang, P., Guex-Crosier, Y. Schematic Interpretation of Indocyanine Green Angiography in Posterior Uveitis Using a Standard Angiographic Protocol. *Ophthalmology 105*, 432-440 (1998).
18. Chen, S. J., Lee, A. F., Lee, F. L., Liu, J. H. Indocyanine Green Angiography of Central Serous Chorioretinopathy. *Zhonghua Yi Xue Za Zhi (Taipei) 62*, 605-613 (1999).
19. Mueller, A. J., Freeman, W. R., Schaller, U. C., Kampik, A., Folberg, R. Complex Microcirculation Patterns Detected by Confocal Indocyanine Green Angiography Predict Time to Growth of Small Choroidal Melanocytic Tumors: MuSIC Report II. *Ophthalmology 109*, 2207-2214 (2002).
20. Haglund, M. M., Berger, M. S., Hochman, D. W. Enhanced Optical Imaging of Human Gliomas and Tumor Margins. *Neurosurgery 38*, 308-317 (1996).
21. Reynolds, J. S., Troy, T. L., Mayer, R. H., Thompson, A. B., Waters, D. J., Cornell, K. K., Snyder, P. W., Sevick-Muraca, E. M. Imaging of Spontaneous Canine Mammary Tumors using Fluorescent Contrast Agents. *Photochem. Photobiol. 70*, 87-94 (1999).
22. Borotto, E., Englender, J., Pourny, J. C., Naveau, S., Chaput, J. C., Lecarpentier, Y. Detection of the Fluorescence of GI Vessels in Rats using a CCD Camera or a Near-infrared Video Endoscope. *Gastrointest. Endosc. 50*, 684-688 (1999).
23. Taggart, D. P., Choudhary, B., Anastasiadis, K., Abu-Omar, Y., Balacumaraswami, L., Pigott, D. W. Preliminary Experience with a Novel Intraoperative Fluorescence Imaging Technique to Evaluate the Patency of Bypass Grafts in Total Arterial Revascularization. *Ann Thorac. Surg. 75*, 870-873 (2003).
24. Still, J. M., Law, E. J., Klavuhn, K. G., Island, T. C., Holtz, J. Z. Diagnosis of Burn Depth using Laser-induced Indocyanine Green Fluorescence: A Preliminary Clinical Trial. *Burns 27*, 364-371 (2001).
25. Chen, J., Tung, C. H., Mahmood, U., Ntziachristos, V., Gyurko, R., Fishman, M. C., Huang, P. L., Weissleder, R. *In Vivo* Imaging of Proteolytic Activity in Atherosclerosis. *Circulation 105*, 2766-2771 (2002).
26. Tung, C. H., Gerszten, R. E., Jaffer, F. A., Weissleder, R. A Novel Near-infrared Fluorescence Sensor for Detection of Thrombin Activation in Blood. *Chembiochem 3*, 207-211 (2002).

27. Marten, K., Bremer, C., Khazaie, K., Sameni, M., Sloane, B., Tung, C. H., Weissleder, R. Detection of Dysplastic Intestinal Adenomas Using Enzyme-sensing Molecular Beacons in Mice. *Gastroenterology 122*, 406-414 (2002).

28. Petrovsky, A., Schellenberger, E., Josephson, L., Weissleder, R., Bogdanov, A., Jr. Near-infrared Fluorescent Imaging of Tumor Apoptosis. *Cancer Res. 63*, 1936-1942 (2003).

29. Achilefu, S., Dorshow, R. B., Bugaj, J. E., Rajagopalan, R. Novel Receptor-targeted Fluorescent Contrast Agents for *In Vivo* Tumor Imaging. *Invest. Radiol. 35*, 479-485 (2000).

References

30. Becker, A., Hessenius, C., Licha, K., Ebert, B., Sukowski, U., Semmler, W., Wiedenmann, B., Grotzinger, C. Receptor-targeted Optical Imaging of Tumors with Near-infrared Fluorescent Ligands. *Nat. Biotechnol. 19*, 327-331 (2001).

31. Tung, C. H., Lin, Y., Moon, W. K., Weissleder, R. A Receptor-targeted Near-infrared Fluorescence Probe for *In Vivo* Tumor Imaging. *Chembiochem 3*, 784-786 (2002).

32. Zaheer, A., Wheat, T. E., Frangioni, J. V. IRDye78 Conjugates for Near-infrared Fluorescence Imaging. *Molecular Imaging 1*, 354-364 (2002).

33. Lamb, T. D. Photoreceptor Spectral Sensitivities: Common Shape in the Long-wavelength Region. *Vision Res. 35*, 3083-3091 (1995).